Supplementary Information to:

The Plastic Ceiling

Opportunities and Limitations of Microbial Carbon Recovery in Crewed Spaceflight

Contents

1 Guide to the Supplementary Information **2**

2 Carbon Accounting Procedure **3**
- 2.1 Basis, Normalization, and Complementarity . . . 3
- 2.2 Crew-Time Normalization . . . 4
- 2.3 Logistics Up-Mass Baseline and Era Scaling . . . 4
- 2.4 Respired Carbon Dioxide and Its Disposition . . . 5
- 2.5 Wet Organic Streams . . . 6
  - 2.5.1 Food Supply and Its Partition . . . 6
  - 2.5.2 Feces, Urine, and Human Detritus . . . 6
  - 2.5.3 Residual Food Waste by Deductive Closure . . . 7
- 2.6 Cellulose-Containing Solids . . . 8
- 2.7 Polymer Streams . . . 8
  - 2.7.1 Soft-Goods Logistics Packaging . . . 8
  - 2.7.2 Packing Foam . . . 9
  - 2.7.3 Food Packaging and Bulk Overwrap Bags . . . 9
  - 2.7.4 Clothing and Hygiene Polymers . . . 10
  - 2.7.5 Partition into Bio-Deconstructable and Recalcitrant Polymer . . . 10
- 2.8 Closure Checks . . . 11
- 2.9 Simplifications and Their Justification . . . 11

3 Bio-Process Sizing Framework **12**
- 3.1 Scope, System Boundary, and Steady-State Assumption . . . 12
- 3.2 Carbon-Stream Interconversion . . . 12
- 3.3 Bioprocess Sizing Chain . . . 13
- 3.4 Scenarios and Models . . . 15
- 3.5 Known Limitations . . . 15

4 Supplementary Figures **17**

1 Guide to the Supplementary Information

The supplementary material accompanying this study is distributed across several files, listed in Supplementary Table 1. This document collects the detailed carbon-accounting procedure, the formulation of the Bio-Process Sizing Framework, and the supplementary figures. The framework itself is additionally supplied as a separate, fully formula-driven workbook, so that it can be inspected, re-run, or cited independently of this document.

Supplementary Table 1: Contents of the supplementary material.

Item	**Format**	**Content**
Supplementary Information	PDF	This document: the detailed carbon-accounting procedure, the formulation of the Bio-Process Sizing Framework, and the supplementary figures.
Supplementary Data 1	XLSX	The Bio-Process Sizing Framework. Formula-driven and directly editable workbook, and the authoritative source for every value reported in the main text: sheet descriptions and the scenario legend (`Description`), physical constants (`Constants`), the carbon stream inventory (`Inputs`), all scenario parameters (`Parameters`), stream interconversion and the allocation matrix (`Routing`), the two bioprocess parameter sets (`Theoretical`, `Empirical`), the route-resolved sizing outputs and global carbon ledger (`Scenarios`), and the inverse sizing case, in which a given installed reactor volume determines processing capacity and the division of carbon between routes competing for one stream (`Volume-Limited`).

2 Carbon Accounting Procedure

2.1 Basis, Normalization, and Complementarity

The carbon accounting was constructed to be fully traceable, algebraically closed under explicitly stated simplifications, and robust to missing manifest-level detail. Three methodological choices follow from those requirements and govern everything below.

First, accounting is rate-based rather than manifest-based. All quantities are expressed per crew member and per year, in kilograms of carbon, and are anchored to crew time in person-years, to logistics-only up-mass rates in metric tons per person-year, and to standardized consumable and waste-generation rates drawn from the NASA *Baseline Values and Assumptions Document* (BVAD)[1] and the primary literature. This is appropriate because the underlying operational processes are steady over the intervals considered, and because BVAD planning values already embed mission heterogeneity. A rate basis also permits variable-throughput items (food) and fixed-throughput items (toothbrushes) to be combined in a single ledger.

Second, soft-goods logistics packaging is represented as a throughput tied to cargo mass rather than as a mass of bags discarded, using the Cargo Transfer Bag Equivalent (CTBE) as the normalizing unit. Accounting in physical bag counts would require a mission-by-mission size distribution and would still not resolve packing efficiency, whereas NASA logistics models treat the CTBE as carrying a packaging mass independent of its contents. This yields a well-defined annual material throughput without requiring a model of container lifetime; container reuse enters separately, as the single steady-state factor described with the polymer partition.

Third, streams are defined so that overlap is structurally impossible. Food adhered to packaging is counted as wet organics and excluded from packaging polymer; cotton in clothing is counted as cellulose and excluded from synthetic clothing polymer; CTB and M-bag textiles are counted as packaging and excluded from clothing and hygiene textiles. Where BVAD aggregates categories in a way that would create overlap, explicit subtraction or category reassignment was performed and is documented at the relevant subsection.

All values refer to a representative crew member, defined as an astronaut of average mass consuming nominal quantities of each supply and producing nominal quantities of each waste.

Where a source reports nominal, lower, and upper values, the nominal value was adopted. The mass of sex-specific items was halved, so that the representative crew member approximates a crew of equal sex ratio.

Several streams lie outside the accounting boundary. Propellant, maintenance and upkeep hardware, experimental payloads, and structural polymers not classed as logistics are excluded by definition. Medical supplies are excluded because their consumption is highly variable and mission-dependent, a limitation the BVAD states explicitly and for which it offers no planning value; consumption is not tracked operationally. Waste-collection hardware and containment bags were judged negligible against the streams retained, as was carbon dioxide respired by rodent payloads, which is both small and intermittent rather than steady-state.

2.2 Crew-Time Normalization

The continuous-habitation record from November 2000 to November 2025 was segmented into five operational eras, each corresponding to a stable baseline crew complement (Supplementary Table 2). Era-specific crew time was computed as the product of mean onboard crew and era duration, the mean including the transient increments that occur during crew handover, and converted from crew-days to crew-years. Summed across eras this gives 132.6 person-years, the quantity used both for per-capita normalization and for lifetime aggregation.

The time-weighted mean crew complement over the record is

$$\bar{N} = \frac{\sum_i N_i t_i}{\sum_i t_i}, \tag{1}$$

where N_i is the mean crew size in era i and t_i its duration in days. Evaluating Eq. (1) over the five eras yields $\bar{N} = 5.29 \pm 0.2$, and this value is used throughout as the crew factor converting per-crew-member rates to absolute station-level fluxes. The stated uncertainty reflects the approximations in era durations, handover lengths, and rotation counts.

2.3 Logistics Up-Mass Baseline and Era Scaling

Logistics-only up-mass is defined as delivered pressurized cargo entering the ISS consumables or equipment inventory that can ultimately contribute to a carbon-bearing waste stream. Propellant

Supplementary Table 2: ISS operational eras used for crew-time normalization. Mean crew includes handover increments. Logistics mass is pressurized cargo excluding propellant (Section 2.3).

Era	Period	Duration (d)	Base crew	Mean crew	Person-years	Logistics (t)	Rate (t/(p·a))
I	Nov 2000 – Feb 2003	821	3	3.12	7.02	36	5.1
II	Feb 2003 – Jul 2006	1246	2	2.08	7.10	30	4.2
III	Jul 2006 – May 2009	1035	3	3.96	11.23	55	4.9
IV	May 2009 – Nov 2020	4202	6	6.12	70.46	314	4.5
V	Nov 2020 – Nov 2025	1847	7	7.27	36.79	113	3.1
Total	**25.07 a**	**9151**		**5.29**	**132.6**	**548**	**4.1**

transferred for reboost is excluded, and for mixed cargo-propellant vehicles, the propellant mass was removed before totaling. Per-vehicle logistics capacities and per-era flight counts were compiled from agency mission records, and the resulting era totals are given in Supplementary Table 2. The lifetime total of approximately 548 t over 25 years corresponds to about 22 t per year.

Era IV (2009–2020) was adopted as the steady-state reference, with $t_4 = 4.5$ t/(person·a). A dimensionless era scaling factor was defined as $S_e = t_e/t_4$, giving $S_{\mathrm{I}} = 1.1333$, $S_{\mathrm{II}} = 0.9333$, $S_{\mathrm{III}} = 1.0889$, $S_{\mathrm{IV}} = 1.0000$, $S_{\mathrm{V}} = 0.6889$, and a person-year-weighted mean $S_{\mathrm{mean}} = 0.9247$. This factor is applied when extending a stream derived for Era IV across the full record, under the explicit assumption that era-to-era variation in up-mass per person-year reflects changing logistics demand rather than changing packaging or container efficiency; the latter is treated separately through the bounded packing cases of Section 2.7.1. The decline in Era V is attributed to improved water and air recycling, better spare-part inventory management, and tighter cargo mass budgeting, rather than to under-supply.

2.4 Respired Carbon Dioxide and Its Disposition

Respired CO_2 was computed from a daily production rate of 1.08 kg CO_2/(person·d) for a representative 82 kg crew member on a heavy exercise regimen[2], giving 394.2 kg CO_2/(person·a). Applying the stoichiometric carbon mass fraction of CO_2, $12/44 = 0.2727$, yields 107.5 kg_C/(person·a). This stream is structurally independent of the logistics material streams and is therefore additive without risk of overlap.

The disposition of scrubbed CO_2 was resolved because it determines the form in which respired carbon leaves the station. CO_2 is removed from cabin air by the Carbon Dioxide Removal Assembly,

the ESA Advanced Closed Loop System, and Vozdukh, and is then either vented directly or reduced in a Sabatier reactor. For steady-state operation, it was assumed that 47% of available CO_2 is routed to Sabatier reduction at 99% conversion. Accordingly, 53% of respired carbon (57.0 kg_C/(person·a)) is vented directly as CO_2; 47% (50.5 kg_C/(person·a)) enters the reactor, of which 99% (50.0 kg_C/(person·a)) is vented as methane and the residual 1% as unreacted CO_2. Product water is retained and electrolyzed, contributing to oxygen recovery, but the carbon is not recovered.

2.5 Wet Organic Streams

2.5.1 Food Supply and Its Partition

The NASA food supply planning value is 2.39 kg/(person·d) as shipped, derived from the maximum six-month rate of food bags opened aboard ISS. Of this, 0.43 kg is packaging (0.40 kg food packet material, 0.03 kg bulk overwrap bag) and 1.96 kg is food, which is 51.3% dry matter and 48.7% water in unopened packets. The food fraction partitions into 1.56 kg consumed, 0.20 kg prepared but wasted, and 0.20 kg never opened.

Dry matter was modeled stoichiometrically as 50% carbohydrate ($C_6H_{12}O_6$), 27.5% fat ($C_5H_9O_2$), and 22.5% protein ($C_6H_{15}O_2N_2$), consistent with the BVAD adhered-food model. The corresponding carbon mass fractions are 0.40, 0.59, and 0.49, giving a weighted dry-matter carbon fraction of 0.472, rounded to 0.47. Annualizing the three subsets gives 137.24, 17.52, and 17.52 kg_C/(person·a) respectively, for a nominal total food supply of 172.28 kg_C/(person·a).

2.5.2 Feces, Urine, and Human Detritus

Fecal and urine masses were taken from BVAD per-day values and annualized, giving 44.90 and 570.13 kg/(person·a) respectively at nominal. The fecal dry-solids fraction was computed from the BVAD solids tables and fecal carbon assumed to be 50% of dry solids[3]; urine carbon was computed from an organic fraction of 3.78% at an assumed carbon content of 13%. This gives 8.07 kg_C/(person·a) for feces and urine combined.

Human detritus comprises sweat solids, skin cells, skin oils, hair, saliva solids, mucus solids, and nails, annualized from BVAD per-day values and assigned carbon by composition proxy: sweat and saliva solids as predominantly water and electrolytes with negligible carbon[4]; skin cells and

nails as 90% keratin and hair as 80% keratin, at a total carbon content of 51%[5, 6]; skin oils as lipid-dominated at 80% carbon[7]; and mucus as 97% water with 1.5% carbon in the solids[8]. The total is 1.724 kg_C/(person·a). Menstrual blood loss was computed from a mean 43.4 mL per cycle[9] over twelve cycles per year, at a whole-blood carbon content of 5.075% derived from a 55:45 plasma-to-cell split, and halved for crew sex ratio, giving 0.014 kg_C/(person·a). These simplifications are acceptable because detritus is a minor contributor relative to the packaging, cellulose, and respiration streams, and uncertainty in its carbon fraction has negligible effect on the total.

2.5.3 Residual Food Waste by Deductive Closure

Residual food waste comprises food never opened, food adhered to package interiors, and plate waste. All three were assigned to wet organics rather than to packaging, which is what prevented adhered food from being implicitly counted as polymer.

The magnitude of this stream was derived deductively rather than measured. At metabolic steady state, and assuming no net change in crew body mass, all carbon in consumed food must leave as respired CO_2 or in a wet organic waste stream:

$$\text{food consumed} \;=\; \text{respired } CO_2 \;+\; \text{wet organic waste.} \tag{2}$$

The right-hand side is fixed by the preceding subsections at $107.5 + 9.8 = 117.3$ kg_C/(person·a), whereas annualizing the supply planning value gives a nominal consumed figure of 137.24 kg_C/(person·a). The difference of 19.94 kg_C/(person·a) cannot be metabolized and is therefore routed to food waste. Adding it to the two explicit waste subsets gives a total residual food waste of $17.52 + 17.52 + 19.94 = 54.98$ kg_C/(person·a), and a nominal wet organics stream, including feces, urine, detritus, and blood, of 64.8 kg_C/(person·a).

This treatment is justified on two grounds. The 2.39 kg planning value is the maximum six-month rate of food bags opened and is not the quantity a representative 82 kg crew member is expected to consume, and food is deliberately supplied in surplus to avoid end-of-mission shortfall[2]. Eq. (2) therefore functions simultaneously as a derivation and as a closure check on the metabolic streams.

2.6 Cellulose-Containing Solids

Cellulosic items were treated as a dedicated stream because they are compositionally distinct from wet organics, being low-moisture fibrous solids, and because they must be separated from synthetic textiles to preserve complementarity with the polymer streams. Cotton and paper were taken as 100% cellulose–non-cellulosic finishes and dyes being negligible against the mass uncertainty in supply rates–and cellulose carbon was computed throughout at $f_C = 0.44$.

Per-item supply rates were taken from the BVAD and from the ISS logistics literature[10, 11, 12, 13]. Cotton in clothing was itemized at 0.207 kg/(person·d), or 75.56 kg/(person·a), giving 33.24 kg_C/(person·a); this figure is net of generalized clothing mass already carried in the CTBE packaging category, which was subtracted explicitly to avoid double counting. Cellulose in hygiene items, comprising towels and wipes at 0.475 kg/(person·d) together with sleeping-bag liners (one per 30 days at 400 g, taken as 100% cotton)[14] and tampons (97.2 g/(person·month) from BVAD, halved for crew sex ratio), totals 78.69 kg_C/(person·a). Per the BVAD, paper is still used extensively aboard ISS for documentation, and the nominal value of 0.0260 kg/(person·d) sums to 4.18 kg_C/(person·a). The cellulose stream carried forward is therefore 116.11 kg_C/(person·a).

2.7 Polymer Streams

2.7.1 Soft-Goods Logistics Packaging

The Era IV crew-normalized logistics rate is 4456.7 kg/(person·a), from 314 t delivered over 4202 days at a mean crew of 6.12, equivalent to 70.46 crew-years. Packaging polymer mass per CTBE was treated as a fixed abstraction independent of contents, comprising 0.83 kg of CTB fabric and 0.10 kg of internal liner, for 0.93 kg polymer per CTBE.

Because the CTBE is a capacity unit rather than a physical container, the number required to deliver a given cargo mass depends on packing efficiency. An effective load of 15.38 kg/CTBE was adopted, corresponding to the legacy planning requirement of 65 CTBE per 1000 kg of pressurized cargo. At the Era IV logistics rate this gives 290 CTBE/(person·a), and hence 269 kg polymer/(person·a); extension across eras follows $N_{e,k} = N_{4,k} S_e$.

CTBE textile was treated as a mixed fabric of 7.5% polyamide, 7.5% polyester, and 85% aramid-dominant material, at carbon mass fractions of 0.637, 0.625, and 0.706 respectively, giving 0.646 kg_C

per CTBE partitioned as 0.044 kg_C polyamide, 0.044 kg_C polyester, and 0.558 kg_C aramid. At the person-year-weighted era scaling, this yields 173.3 kg_C/(person·a), partitioned as 11.9 kg_C polyamide, 11.7 kg_C polyester, and 149.7 kg_C aramid.

Packing efficiency is the dominant uncertainty in this stream, which supplies roughly half of all recalcitrant polymer carbon. The certified mass-limited maximum of 26.81 kg/CTBE and the historically observed volume-limited loading of 10.26 kg/CTBE would give 99 and 259 kg_C/(person·a) in place of the adopted 173.3, a range extending a factor of 1.75 below the reported figure and 1.5 above it.

2.7.2 Packing Foam

Foam masses were taken from CTB packing-foam inventory data supplied by the ISS Cargo Mission Contract program (Leidos, personal communication), averaged over 2022–2025. Two grades dominated the total and were retained: Plastazote LD45 FR, a flame-retarded crosslinked low-density polyethylene, at 7.57 kg/(person·a); and ZOTEK F30, a closed-cell crosslinked poly(vinylidene fluoride), at 31.74 kg/(person·a). Polymer identities were taken from manufacturer technical data sheets and confirmed by the program technical lead[15].

Carbon mass fractions were computed from repeat-unit stoichiometry assuming pure homopolymer composition: –(CH_2–CH_2)– for polyethylene (M = 28 g mol^{-1}, w_C = 24/28 = 0.857) and –(CH_2–CF_2)– for PVDF (M = 64 g mol^{-1}, w_C = 24/64 = 0.375). Integer atomic masses were used; substituting IUPAC standard atomic weights changes the result by less than 0.1%. The flame-retardant additive content of Plastazote LD45 FR is not specified by the manufacturer, so its mass was assigned in full to polyethylene, giving an upper bound on polyethylene-derived carbon. This yielded 6.49 kg_C/(person·a) from the polyethylene foam and 11.90 kg_C/(person·a) from the PVDF foam, for a total foam-derived carbon flux of 18.4 kg_C/(person·a).

2.7.3 Food Packaging and Bulk Overwrap Bags

Food packaging plastic was treated as a polymer stream complementary to the residual food organics that adhere to it. From the 2.39 kg/(person·d) food planning value, 0.40 kg is packet material and 0.03 kg bulk overwrap bag (BOB). Packet material was taken as equal thirds polyethylene, polypropylene, and polystyrene per the BVAD, at carbon mass fractions of 0.856, 0.856, and 0.923,

giving a nominal 128.27 kg_C/(person·a). BOB composition was taken as 25% polyethylene, 55% PET, and 20% aluminum, giving 2.36 kg_C/(person·a) from polyethylene and 3.76 kg_C/(person·a) from PET.

2.7.4 Clothing and Hygiene Polymers

Clothing supply was taken at 0.377 kg/(person·d) net of CTB mass[10], itemized by garment and assigned polymer composition by subcategory[12]. The resulting carbon contributions are 22.81 (PET), 6.07 (polyamide), 3.11 (aramid), 4.75 (polyurethane/elastane), 1.97 (styrene-butadiene rubber), and 1.48 (ethylene-vinyl acetate) kg_C/(person·a), for a total clothing polymer carbon of 40.19 kg_C/(person·a), of which 28.88 is bio-deconstructable (PET and polyamide) and 11.31 recalcitrant.

Hygiene items were partitioned by material type into cellulose, treated in the preceding section, and polymer. Polymer contributions are 7.30 (PET), 18.21 (polyethylene), 10.99 (polypropylene), 3.05 (polycarbonate), and 0.23 (polyamide) kg_C/(person·a), for a total of 39.78 kg_C/(person·a), of which 7.53 is bio-deconstructable and 32.25 recalcitrant. Nitrile gloves were accounted separately at 0.016 kg/(person·d), taken as a 35:65 acrylonitrile-butadiene copolymer at carbon mass fractions of 0.679 and 0.888, giving 4.76 kg_C/(person·a), all recalcitrant.

2.7.5 Partition into Bio-Deconstructable and Recalcitrant Polymer

Polymer carbon was partitioned by whether the backbone carries a hydrolyzable linkage for which enzymatic depolymerization has been demonstrated. Polyesters and aliphatic polyamides were classed as bio-deconstructable, and polyolefins, polystyrene, polycarbonate, aromatic polyamides (aramids), fluoropolymers, and elastomers as recalcitrant. A reuse rate of 25% is assumed for cargo transfer bags under steady-state operations, based on operational experience of ISS cargo handling and stowage (K.H.R.), so only 75% of CTB-derived polymer mass reports to the waste stream and to the bioprocessing inlet. The factor is applied to all CTB-derived polymer, aramid, polyamide, and polyester alike. Summing across the streams above gives 42.6 kg_C/(person·a) of polyester, 15.2 kg_C/(person·a) of polyamide, and 309.6 kg_C/(person·a) of recalcitrant polymer (Supplementary Fig. 1).

2.8 Closure Checks

Three checks constrain the accounting. Internal complementarity is enforced by construction: any quantity that could be assigned to two categories is allocated to exactly one by rule, and each such rule is documented at the relevant subsection. Independently, the metabolic streams close through Eq. (2), which fixes wet organic waste against respired CO_2 and food supply rather than leaving it to be estimated. A third check is available downstream, where lifetime terminal carbon computed from the disposal side and lifetime up-linked carbon computed from the supply side are derived independently and agree to within 0.04 kg across an 87 t total, as reported in Figure 2 of the main text.

2.9 Simplifications and Their Justification

Representative polymer-class carbon fractions were used rather than part-number-specific formulations, because polymer class dominates the elemental carbon fraction and is sufficient for the bio-deconstructable against recalcitrant differentiation that the analysis requires. Residual food carbon was treated with a BVAD-consistent stoichiometric diet model and a rounded dry-matter carbon fraction of 0.47, because diet composition varies less than the mass uncertainty in adhered-food and discard rates, and rounding avoids false precision while preserving consistency across the wet organic calculations. CTBE throughput was computed from a single stated packing efficiency rather than modeled mission by mission, because mission-specific packing behavior is poorly constrained by public data; the sensitivity of that choice is given in Section 2.7.1.

3 Bio-Process Sizing Framework

3.1 Scope, System Boundary, and Steady-State Assumption

The framework resolves carbon only. Water, nitrogen, phosphorus, trace nutrients, and energy are outside the system boundary, and no attempt is made to close balances in those elements. The station is treated as operating at quasi-steady state, so that accumulation of carbon within the habitat is negligible relative to throughput, and annual inputs can be balanced directly against outputs and transformations. All bioprocesses are evaluated under standard aqueous conditions, at the reference temperature and pressure recorded on the `Constants` and `Parameters` sheets of Supplementary Data 1.

Carbon accounting was performed per crew member and per year, and scaled to absolute annual fluxes by the time-weighted mean crew complement (`Inputs` sheet). Consequently, every quantity in this supplement is an annualized mean; start-up transients, resupply cadence, crew handover peaks, and off-nominal operations were not represented.

3.2 Carbon-Stream Interconversion

Raw waste streams are not all directly bioavailable, so three thermochemical or biochemical interconversion steps precede the biological stage: anaerobic digestion of wet organics, pyrolysis of recalcitrant plastics, and Sabatier methanation of the pooled carbon dioxide. Their governing parameters are given on the `Routing` sheet of Supplementary Data 1, together with the resulting pooled streams. Each pooled stream is then divided among the conversion mechanisms that can accept it, in the proportions given by the allocation matrix on the same sheet.

Interconversion is resolved in a single forward pass. Products of one step are not returned to the inlet of another, and no iteration to a fixed point is performed. This keeps the model transparent and analytically tractable, but means that any recycle loop a real plant would operate, for example, returning Sabatier product water or unconverted pyrolysis gas, is not credited.

The single largest structural difference between the two routing scenarios lies in the pyrolysis step. The Baseline scenario routes a small fraction of the recalcitrant plastic stream through plasma pyrolysis, whereas the Aspirational scenario routes the great majority through microwave-assisted

pyrolysis, which is represented with a higher carbon conversion efficiency and a product distribution shifted toward methane at the expense of carbon monoxide and carbon dioxide (`Routing` sheet). The scenarios also differ in the share of wet organics digested, 90% against 50%, and in the fraction of the pooled carbon dioxide methanated in the Sabatier step, 50% against 95%; the latter leaves little carbon dioxide for the autotrophic routes in the Aspirational scenario and supplies half of its methane.

3.3 Bioprocess Sizing Chain

Each conversion route is characterized by four quantities: the volumetric carbon processing rate r_C, the volumetric carbon processing capacity C_{cap}, the biomass volumetric productivity P_V, and the biomass yield on carbon $Y_{X/C}$. Capacity follows from rate-by-unit conversion, and the two sizing outputs (required reactor volume V and annual biomass output X) follow from the carbon stream allocated to that route:

$$C_{\mathrm{cap}} \;=\; r_C \,\frac{t_{\mathrm{a}}}{1000}, \qquad V \;=\; \frac{C_{\mathrm{stream}}}{C_{\mathrm{cap}}}, \qquad X \;=\; C_{\mathrm{stream}}\, Y_{X/C}, \tag{3}$$

where t_{a} is the number of days per year (`Constants` sheet) and the factor of 1000 converts grams to kilograms. Equation (3) is the whole of the sizing chain: the modeling effort sits entirely in r_C and $Y_{X/C}$, which are what distinguish the two models. The resulting distribution of reactor volume across routes is shown in Supplementary Fig. 3.

In the Theoretical model, r_C is derived from whichever physical process limits the route: light delivery for photoautotrophy, gas–liquid mass transfer for lithoautotrophy, acetogenesis, and methanotrophy, oxygen transfer for aerobic heterotrophy, and hydrolysis or depolymerization kinetics for cellulose and the polymers. The limiter for each route is named on the `Theoretical` sheet. In the Empirical model, P_V and $Y_{X/C}$ are taken from the reported performance of specific organisms, and r_C and C_{cap} follow from them (`Empirical` sheet).

For the gas-transfer-limited routes, the volumetric transfer rate of species i is

$$N_i \;=\; u\, k_L a\, H_i^{cp}\, p_i, \tag{4}$$

with $k_L a$ the volumetric mass-transfer coefficient, H_i^{cp} the Henry's-law solubility at the operating temperature, p_i the partial pressure of i in the sparged gas, and u the fraction of transferred gas the culture utilizes. Carbon uptake then follows from whichever reactant limits the mechanism, converted to a mass basis by the molar mass of carbon M_C: $r_C = M_C N_{\mathrm{CO}}$ for the acetogen; $r_C = M_C \min\!\left(N_{\mathrm{CH_4}},\, N_{\mathrm{O_2}}/\alpha_{\mathrm{O_2/CH_4}}\right)$ for the methanotroph, with $\alpha_{\mathrm{O_2/CH_4}}$ the oxygen demand per methane oxidized; and

$$r_C \;=\; M_C \min\!\left(N_{\mathrm{CO_2}},\; \frac{\min(N_{\mathrm{H_2}},\, 2N_{\mathrm{O_2}})}{n_{\mathrm{H_2/C}}}\right) \tag{5}$$

for the aerobic lithoautotroph, whose electron donor is supplied at the lesser of the hydrogen transfer rate and twice the oxygen transfer rate, and where $n_{\mathrm{H_2/C}}$ is the hydrogen demand per carbon fixed. The aerobic heterotrophic routes on volatile fatty acids and wet organics are oxygen-transfer-limited, $r_C = M_C N_{\mathrm{O_2}}/\alpha_{\mathrm{O_2/C}}$; the mixotrophic route shares this rate and differs only in its yield.

The photoautotrophic route is light-limited rather than transfer-limited, and is sized from the areal biomass productivity P_A and the illuminated area per unit volume A/V:

$$r_C \;=\; f_{C,X}\, P_A\, \frac{A}{V}, \tag{6}$$

where $f_{C,X}$ is the carbon mass fraction of biomass. This is the one route whose r_C is expressed on a biomass-carbon basis rather than as a substrate uptake rate, so the identity $P_V = r_C Y_{X/C}$, which holds for every other route in both layers, does not hold here; the photoautotrophic reactor is correspondingly sized as though all carbon taken up were fixed.

The solid substrates follow first-order hydrolysis or depolymerization kinetics on the carbon loading C_L, attenuated by a high-solids penalty:

$$r_C \;=\; u_s\, k\, C_L\, \phi, \qquad \phi \;=\; \max(0,\; 1 - \beta \max(0,\; \mathrm{TS} - \mathrm{TS_{ref}}))\,, \qquad \mathrm{TS} \;=\; \frac{C_L}{1000 f_C}, \tag{7}$$

with k the first-order rate constant for the substrate, u_s a utilization factor, f_C the carbon mass fraction of the substrate, and β the penalty slope above the reference total-solids fraction $\mathrm{TS_{ref}}$. The anaerobic digestion unit is not rate-limited in this sense and is sized instead on its slurry carbon loading and residence time, $r_C = C_{\mathrm{AD}}/\tau_{\mathrm{AD}}$. All parameters are set on the `Parameters` sheet of

Supplementary Data 1, and the limiter applying to each route is named on the `Theoretical` sheet.

3.4 Scenarios and Models

Projections are reported over a two-by-two design. The *scenario* axis (Baseline versus Aspirational) varies the routing and operating parameters on the `Parameters` sheet: how much of each stream is made accessible, and how aggressively each process is operated. The *model* axis (Theoretical versus Empirical) varies where the bioprocess parameters come from, as described above. The two axes are independent, so each of the four combinations is a self-consistent parameterization rather than a scenario in the narrative sense. Carbon routed and biomass produced under each are shown in Supplementary Fig. 2.

3.5 Known Limitations

Several simplifications are deliberate and bound the interpretation of the results.

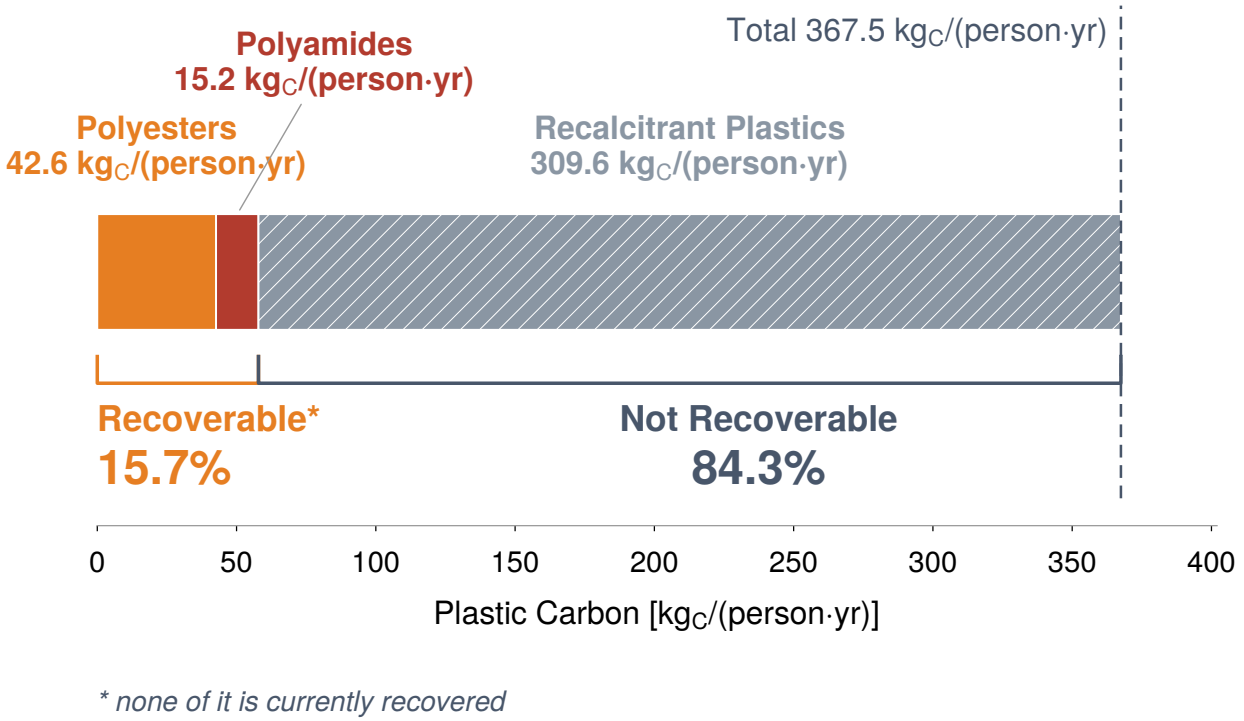
Three rate and yield corrections apply to the Theoretical layer and not to the Empirical layer, whose measured parameters embed them implicitly. Henry's-law solubilities are van 't Hoff-corrected from the tabulated 298.15 K reference to the operating temperature T_{op}, whose default is 303.15 K; setting $T_{\mathrm{op}} = 298.15$ K evaluates the model at the tabulated reference condition. Growth carries a Pirt-type maintenance penalty, parameterized by a growth rate μ_{growth} and a maintenance coefficient $m_{C,\mathrm{maint}}$, which lowers the observed assimilation fraction at low growth rate. A high-solids penalty reduces solid-substrate rates above a total-solids threshold. All three are set on the `Parameters` sheet. Because they apply to one layer only, these corrections bear directly on the relationship between the two.

The two layers are not nested, and neither is intended as a bound on the other. They are two independent estimates of the same quantity, derived from different premises, and their agreement is therefore a check on both: where they converge, the underlying assumptions are mutually corroborated, and where they diverge, the divergence localizes the assumption at fault. Under Baseline routing, the two agree to within a kilogram per year, at 1,693 kg/yr theoretical against 1,694 kg/yr empirical. Under Aspirational routing, the Theoretical layer is the higher of the two, at 2,919 against 2,759 kg/yr, owing to the wet-organic routes the Empirical layer does not resolve and to depolymerization-limited rates no reported chassis yet attains, partly offset by cellulose.

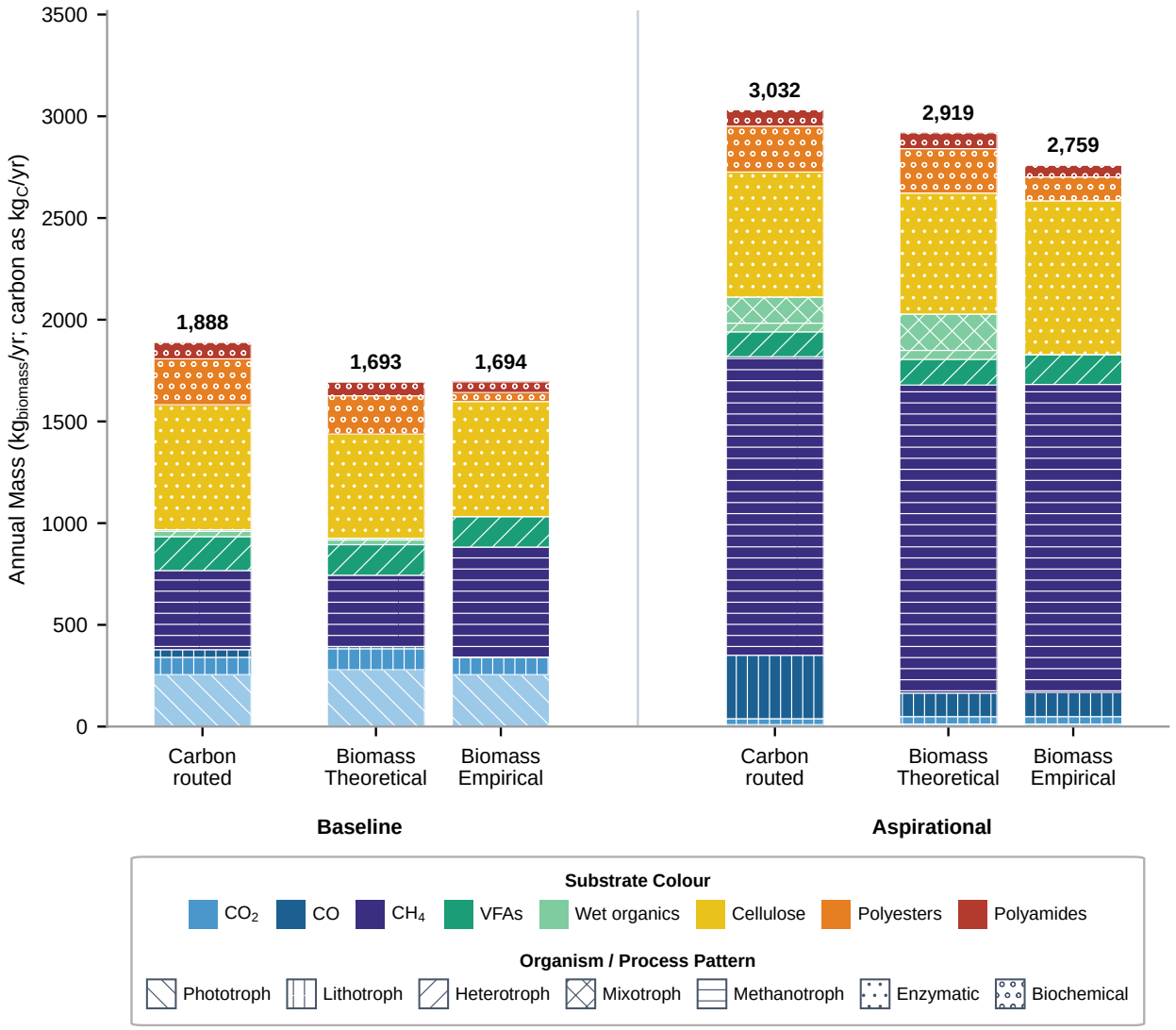
Where an empirical yield was assumed rather than measured, the corresponding theoretical assimilation fraction is used, so that a difference between the two layers reflects the data rather than the bookkeeping.

The organism and literature source underlying every empirical parameterization are recorded in the `Chassis / Reference` column of the `Empirical` sheet. The sources cover photoautotrophy[16, 17], aerobic lithoautotrophy[18, 19], acetogenesis[20, 21], methanotrophy[22, 23, 24], heterotrophy on volatile fatty acids[25, 26], anaerobic digestion[27, 28, 29], cellulose[30, 31], polyesters[32, 33], and polyamides[34, 35, 33]. Every parameterization is drawn from a named strain in a single study. The aerobic heterotrophic and mixotrophic wet-organic routes have no empirical parameterization at all, since no single organism has been reported that represents the mixed cultures they assume; the mixotrophic route inherits the aerobic heterotrophic yield with a scenario-dependent uplift and is therefore unparameterized for the same reason. Both return #N/A rather than zero and are excluded from the empirical totals, which is the largest single source of the divergence between the two layers under Aspirational routing.

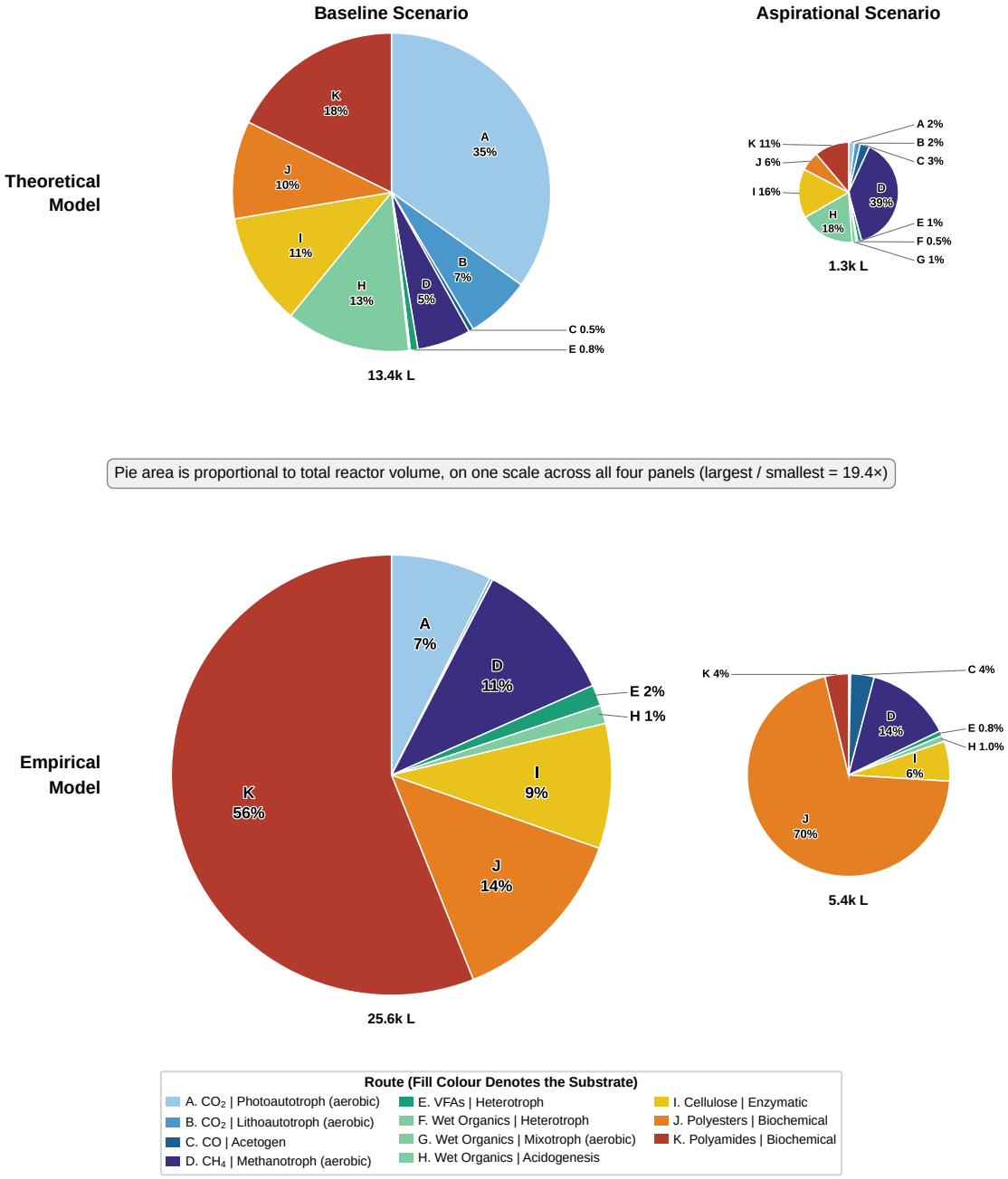
4 Supplementary Figures



Supplementary Figure 1: **Recoverable and non-recoverable plastic carbon.** Annual plastic-carbon inventory of one crew member, partitioned by whether the polymer backbone carries a hydrolyzable linkage for which enzymatic depolymerization has been demonstrated. Fill color identifies the two recoverable polymer classes as in the main-text figures; the recalcitrant fraction is drawn in neutral gray and hatched, marking it as carbon for which the present framework provides no biological route. The bracket beneath divides the bar at that boundary and gives each side as a percentage of the total, with the total itself marked by the dashed rule at the right. The asterisk records that the recoverable fraction is an upper limit on what biology could address rather than a description of current practice: no route assumed here is operated aboard ISS, and none of this carbon is recovered.



Supplementary Figure 2: **Scenario-level carbon routing and biomass output.** Annual routed carbon (as kg$_C$/yr) and the corresponding microbial biomass output (kg/yr) for the Baseline and Aspirational scenarios, each under the Theoretical and Empirical sizing models; the scenario-level aggregate of the route-resolved main-text data. Bars are colored by substrate and hatched by organism/process class (keys below); the CO_2 key is two-toned to distinguish photoautotrophic from lithoautotrophic fixation. Route-resolved values are from the `Bio-Process Sizing Framework` (Supplementary Data 1).



Supplementary Figure 3: **Reactor-volume distribution by bioprocess.** Comparison of sizing model and routing scenarios. Pie area (not radius) is proportional to the total reactor volume that case requires, so a pie of half the diameter denotes a quarter of the volume. The in-figure note states the single area scale and the ratio of the largest case to the smallest, and each pie prints its own total above it. Because that one scale spans all four panels, areas are directly comparable throughout, between scenarios within a model, and between models within a scenario alike. Every wedge is one conversion route, where its angle gives that route's share of its own case total, its fill identifies the substrate consumed, and the letter within it keys to the route legend below, which also carries the substrate key. Wedges too narrow for an interior label carry leader labels outside the rim; six slivers below 0.3% are left unlabeled. Route letters are as in Fig. 4 of the main text. Exact values are tabulated route by route in the `Scenarios` sheet of Supplementary Data 1.

References

[1] Ewert, M. K., Chen, T. T. & Powell, C. D. Life Support Baseline Values and Assumptions Document. NASA Technical Publication, NASA Johnson Space Center (2022). NTRS 20210024855. Cited throughout as BVAD.

[2] Ewert, M. K. & Stromgren, C. Astronaut mass balance for long duration missions. In *49th International Conference on Environmental Systems*, ICES-2019-126 (Boston, MA, 2019).

[3] Rose, C., Parker, A., Jefferson, B. & Cartmell, E. The Characterization of Feces and Urine: A Review of the Literature to Inform Advanced Treatment Technology. *Critical Reviews in Environmental Science and Technology* **45**, 1827–1879, DOI: 10.1080/10643389.2014.1000761 (2015).

[4] Baker, L. B. Physiology of sweat gland function: The roles of sweating and sweat composition in human health. *Temperature* **6**, 211–259, DOI: 10.1080/23328940.2019.1632145 (2019).

[5] Zuniga, K. *et al.* Keratin Promotes Differentiation of Keratinocytes Seeded on Collagen/Keratin Hydrogels. *Bioengineering* **9**, 559, DOI: 10.3390/bioengineering9100559 (2022).

[6] Baswan, S. *et al.* Understanding the formidable nail barrier: A review of the nail microstructure, composition and diseases. *Mycoses* **60**, 284–295, DOI: 10.1111/myc.12592 (2017).

[7] Picardo, M., Ottaviani, M., Camera, E. & Mastrofrancesco, A. Sebaceous gland lipids. *Dermato-Endocrinology* **1**, 68–71, DOI: 10.4161/derm.1.2.8472 (2009).

[8] Fahy, J. V. & Dickey, B. F. Airway Mucus Function and Dysfunction. *New England Journal of Medicine* **363**, 2233–2247, DOI: 10.1056/NEJMra0910061 (2010).

[9] Hallberg, L., Högdahl, A.-M., Nilsson, L. & Rybo, G. Menstrual Blood Loss–A Population Study: Variation at different ages and attempts to define normality. *Acta Obstetricia et Gynecologica Scandinavica* **45**, 320–351, DOI: 10.3109/00016346609158455 (1966).

[10] Leach, H. & Ewert, M. Analysis of Historical International Space Station Logistical Mass Delivery. In *2021 IEEE Aerospace Conference (50100)*, 1–9, DOI: 10.1109/AERO50100.2021.9438212 (IEEE, Big Sky, MT, USA, 2021).

[11] Lynch, C. S. *et al.* A Historical Review of Logistics Mass and Crew Time Demands for ISS Operations. In *53rd International Conference on Environmental Systems*, ICES-2024-132 (Louisville, KY, 2024).

[12] Lynch, C. S., Goodliff, K. E., Stromgren, C., Vega, J. & Ewert, M. K. Logistics Rates and Assumptions for Future Human Spaceflight Missions Beyond LEO. In *ASCEND 2023*, DOI: 10.2514/6.2023-4617 (American Institute of Aeronautics and Astronautics, 2023).

[13] Ichimura, S. & Yamashiki, Y. A. Assessment of the physical and psychological aspects of the current life support system on the International Space Station for sustainable space exploration. *Frontiers in Space Technologies* **5**, DOI: 10.3389/frspt.2024.1461389 (2025).

[14] Maryatt, B. W. Improvements to On-Orbit Sleeping Accommodations. Tech. Rep., NASA Johnson Space Center (2019). NTRS 20190027189; report JSC-E-DAA-TN68145.

[15] Zotefoams plc. Technical Data Sheets: Plastazote LD45 FR and ZOTEK F30. Manufacturer technical literature; polymer identities confirmed by the ISS Cargo Mission Contract technical lead (Leidos, personal communication).

[16] Chunzhuk, E. A. *et al.* The Influence of Elevated CO2 Concentrations on the Growth of Various Microalgae Strains. *Plants* **12**, 2470, DOI: 10.3390/plants12132470 (2023).

[17] Fu, W. *et al.* Maximizing biomass productivity and cell density of *Chlorella vulgaris* by using light-emitting diode-based photobioreactor. *Journal of Biotechnology* **161**, 242–249, DOI: 10.1016/j.jbiotec.2012.07.004 (2012).

[18] Ma, C. *et al.* High-efficiency CO_2 fixation and single-cell protein production in *Cupriavidus necator* via ARTP-driven metabolic rewiring. *Green Chemistry* **28**, 4550–4563, DOI: 10.1039/D5GC05791D (2026).

[19] Tanaka, K., Ishizaki, A., Kanamaru, T. & Kawano, T. Production of poly(D-3-hydroxybutyrate) from CO_2, H_2, and O_2 by high cell density autotrophic cultivation of *Alcaligenes eutrophus*. *Biotechnology and Bioengineering* **45**, 268–275, DOI: 10.1002/bit.260450312 (1995).

[20] Heffernan, J. K. *et al.* Enhancing CO2-Valorization Using *Clostridium autoethanogenum* for Sustainable Fuel and Chemicals Production. *Frontiers in Bioengineering and Biotechnology* **8**, 204, DOI: 10.3389/fbioe.2020.00204 (2020).

[21] Ingelman, H. *et al.* Autotrophic adaptive laboratory evolution of the acetogen *Clostridium autoethanogenum* delivers the gas-fermenting strain LAbrini with superior growth, products, and robustness. *New Biotechnology* **83**, 1–15, DOI: 10.1016/j.nbt.2024.06.002 (2024).

[22] Harwood, J. H. & Pirt, S. J. Quantitative Aspects of Growth of the Methane Oxidizing Bacterium *Methylococcus capsulatus* on Methane in Shake Flask and Continuous Chemostat Culture. *Journal of Applied Bacteriology* **35**, 597–607, DOI: 10.1111/j.1365-2672.1972.tb03741.x (1972).

[23] Jeong, J. *et al.* A highly efficient and versatile genetic engineering toolkit for a methanotroph-based biorefinery. *Chemical Engineering Journal* **453**, 139911, DOI: 10.1016/j.cej.2022.139911 (2023).

[24] Jang, N. *et al.* High Cell-Density Cultivation of *Methylococcus capsulatus* Bath for Efficient Methane-Derived Mevalonate Production. *Journal of Agricultural and Food Chemistry* **71**, 4924–4931, DOI: 10.1021/acs.jafc.3c00286 (2023).

[25] Kolouchová, I., Schreiberová, O., Sigler, K., Masák, J. & Řezanka, T. Biotransformation of volatile fatty acids by oleaginous and non-oleaginous yeast species. *FEMS Yeast Research* fov076, DOI: 10.1093/femsyr/fov076 (2015).

[26] Gao, R. *et al.* Enhanced lipid production by *Yarrowia lipolytica* cultured with synthetic and waste-derived high-content volatile fatty acids under alkaline conditions. *Biotechnology for Biofuels* **13**, 3, DOI: 10.1186/s13068-019-1645-y (2020).

[27] Heo, N. H., Park, S. C. & Kang, H. Effects of Mixture Ratio and Hydraulic Retention Time on Single-Stage Anaerobic Co-digestion of Food Waste and Waste Activated Sludge. *Journal of Environmental Science and Health, Part A* **39**, 1739–1756, DOI: 10.1081/ESE-120037874 (2004).

[28] Lim, S.-J., Choi, D. W., Lee, W. G., Kwon, S. & Chang, H. N. Volatile fatty acids production from food wastes and its application to biological nutrient removal. *Bioprocess Engineering* **22**, 543–545, DOI: 10.1007/s004499900109 (2000).

[29] Lim, S.-J. *et al.* Anaerobic organic acid production of food waste in once-a-day feeding and drawing-off bioreactor. *Bioresource Technology* **99**, 7866–7874, DOI: 10.1016/j.biortech.2007.06.028 (2008).

[30] Poulsen, H. V., Willink, F. W. & Ingvorsen, K. Aerobic and anaerobic cellulase production by *Cellulomonas uda*. *Archives of Microbiology* **198**, 725–735, DOI: 10.1007/s00203-016-1230-8 (2016).

[31] Koyama, Y., Zhao, R., Ike, M. & Tokuyasu, K. *Candida utilis* assimilates oligomeric sugars in rice straw hydrolysate via the Calcium-Capturing-by-Carbonation (CaCCO) process for glutathione- and cell-biomass production. *Bioresource Technology* **172**, 413–417, DOI: 10.1016/j.biortech.2014.08.097 (2014).

[32] Freund, D. *et al.* A synthetic bacterium that degrades and assimilates poly(ethylene terephthalate). bioRxiv, DOI: 10.1101/2025.09.28.673679 (2025). Preprint.

[33] Czajka, J. J. *et al.* Tuning a high performing multiplexed-CRISPRi *Pseudomonas putida* strain to further enhance indigoidine production. *Metabolic Engineering Communications* **15**, e00206, DOI: 10.1016/j.mec.2022.e00206 (2022).

[34] Oulidi, O. *et al.* Enhancing and hindering biodegradation: A comparative study on polyamide 6 reinforced with bio-fillers (peanut shell, olive pomace, and plaster). *Sustainable Chemistry for the Environment* **7**, 100116, DOI: 10.1016/j.scenv.2024.100116 (2024).

[35] de Witt, J. *et al.* Upcycling of polyamides through chemical hydrolysis and engineered *Pseudomonas putida*. *Nature Microbiology* **10**, 667–680, DOI: 10.1038/s41564-025-01929-5 (2025).